Available online at www.sciencedirect.com
SCIENCE DIRECT®
Mathematical and Computer Modelling 41 (2005) 1055–1070
MATHEMATICAL AND COMPUTER MODELLING
www.elsevier.com/locate/mcm

Molecular Dynamics Simulations of Tubulin Structure and Calculations of Electrostatic Properties of Microtubules

J. A. TUSZYŃSKI, J. A. BROWN, E. CRAWFORD, E. J. CARPENTER
Department of Physics, University of Alberta, Edmonton AB, Canada, T6G 2J1
M. L. A. NIP
Department of Biochemistry, Université de Montréal, Montréal QC, Canada H3C 3J7
J. M. DIXON
Physics Department, University of Warwick, Coventry, U.K., CV4 7AL
M. V. SATARIĆ
Faculty of Technical Sciences, University of Novi Sad, 21000 Serbia

Abstract— We present the results of molecular dynamics computations based on the atomic resolution structure of tubulin. Values of net charge, charge distribution and dipole moment components are obtained for the tubulin heterodimer. Physical consequences of these results are discussed for microtubules in terms of the effects on test charges, test dipoles, and neighboring microtubules.

1. INTRODUCTION

Microtubules (MTs) are protein filaments of the cytoskeleton [1] with their outer diameter roughly 23 nm, and a hollow interior with a diameter of roughly 15 nm (see Figure 1). Their lengths vary but commonly reach 5–10 μm dimensions. They are composed of 12 to 17 protofilaments when self-assembled in vitro and almost exclusively of 13 protofilaments in vivo. These protofilaments are strongly bound internally and are connected via weaker lateral bonds to form a sheet that is wrapped up into a tube in the nucleation process [2].

MTs are found in nearly all eukaryotic cells and they perform a variety of key cellular functions. In addition, to providing rigidity and structural integrity to a living cell, they serve as tracks for motor protein transport. They also form the core of cilia and flagella which beat in a coordinated manner to either move objects along the cell membrane or to propel the cell through its environment. Perhaps most importantly, microtubules form mitotic spindles that segregate chromosomes during cell division.

In general, there are three types of action modes of chemical antitumor compounds, namely:

(a) DNA targeting compounds that kill the cell by destroying or blocking the use of its genetic material,

This research was supported by grants from NSERC and MITACS-MMPD. Discussions with Sackett of NIH are gratefully acknowledged. Satarić and Dixon would like to thank the staff of the Theoretical Physics Institute of the University of Alberta for all their kindness during their visits.

0895-7177/05/$ - see front matter Typeset by AMS-TEX
doi:10.1016/j.mcm.2005.05.002

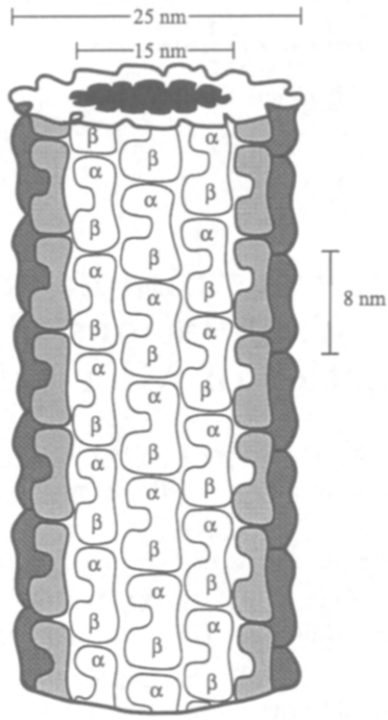

Figure 1. A section of a typical microtubule demonstrating the helical nature of its construction and the hollow interior which is filled with cytoplasm. Each vertical column is known as a protofilament and the typical MT has 13 protofilaments.

(b) compounds which inhibit normal cell functions, and
(c) the so-called spindle poisons which block the mitosis by interfering with the normal behavior of microtubules.

All the above-mentioned chemicals are very toxic. However, one interesting feature of the spindle poison compounds is that they more specifically target fast dividing cells, which is a particular property of cancerous cells. There are two ways by which the spindle poisons can block the mitosis. First, colchicine and vinblastine block the mitosis by preventing the formation of the mitotic spindle. In fact, they inhibit the polymerization of tubulin into microtubules. Second compounds such as taxol and rhazinilam stop the mitosis between the metaphase and the anaphase. They do so by stabilizing the microtubule polymer through binding to tubulin at specific locations as shown in Figure 3. Since the depolymerization is blocked making the microtubules static, the chromosomes cannot migrate toward the poles and cell division cannot be accomplished. It is our belief that analyzing some key physical properties of tubulin and microtubules such as their electrical charge and dipole distributions, we will gain important insights into the mechanism of cell division and possible means of controlling it via sophisticated physical and chemical agents.

The general structure of MTs has been well established experimentally [3,4]. A small difference between the α and β monomers of tubulin allows the existence of several lattice types (see Figure 2). Moving around the MT in a left-handed sense, protofilaments of the A lattice have a vertical shift of 4.92 nm upwards relative to their neighbors. In the B lattice this offset is only 0.92 nm because the α and β monomers have switched positions in alternating filaments. This change results in the development of a structural discontinuity in the B lattice known as a seam [4,5]. In addition, Chrétien *et al.* [6] observed that, the protofilament number need not be conserved along the length of a microtubule leading to the emergence of structural defects in the lattice. Furthermore, Sosa *et al.* [7] showed evidence of more than one seam in microtubules.

The idea that protofilaments have flexible connections, allowing for the presence of defects [8], could explain the anti-parallel alignment of protofilaments in the presence of Zn^{2+} ions. The zinc ion may favor one orientation for hydrophobic bonding. This is also consistent with the

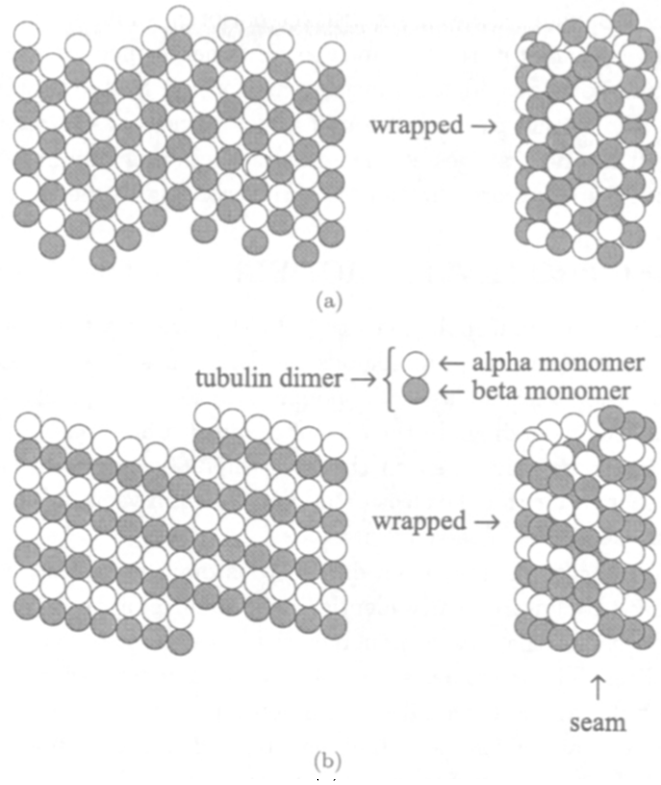

Figure 2. The 13A and 13B MT lattices: (a) in the A lattice, perfect helical spirals are formed. (b) in the B lattice, there is a structural discontinuity known as the seam.

observation of MT assembly in which a seam appears to "zip up" the cylinder behind the assembly edge [2].

In 1998 Nogales *et al.* [9] reported crystallization of tubulin in the presence of zinc ions. Their results were made available through the Protein Data Bank (PDB) [10] (PDB entry: 1TUB) which allowed us to view the three-dimensional atomic resolution structure of tubulin (see Figure 3) using RasMol [11]. Each tubulin monomer is composed of more than 400 amino acids and, in spite of their similarity, slight folding differences can be seen. It is worth stressing that several different versions of both tubulin α and β forms exist an are called isotypes [12] when found in

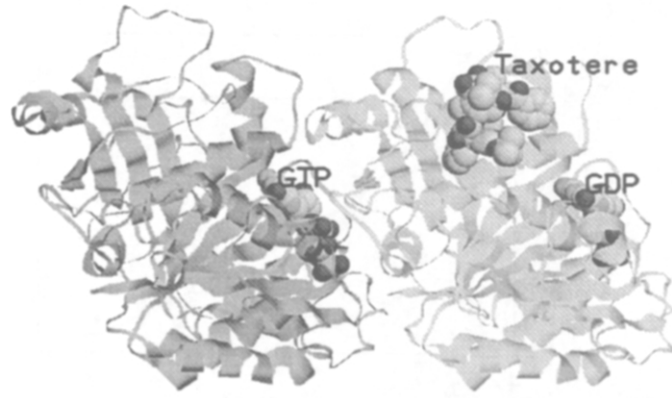

Figure 3. A ribbon diagram of the tubulin molecule produced from the [9] crystallographic data shows the similarity between the α-subunit (up half) and the β-subunit (lower half). The stick outlines near the base of each subunit indicate the location of GTP when bound.

the same organism. In humans at least six distinct α isotypes and seven β isotypes of tubulin have been identified. What is intriguing and, so far, unexplained, is the correlation between localization of certain isotypes and the functions performed by microtubules assembled from them. For example, the β_1 and β_4 are not found in cell nuclei but are present along with β_2 in the mitotic spindle. It has been suggested that, the interaction of tubulin with extrinsic proteins may direct the architecture and organization of MTs according to the isotypes used [13].

2. ELECTROSTATIC MODELLING OF TUBULIN

The method of distributed multipole analysis (DMA) provides a fairly accurate means of calculating the electrostatic field around a biomolecule. Diatomics, triatomics, and tetratomics are described to high precision with the use of monopoles, dipoles and quadrupoles providing an accurate picture of molecular bonding. In the case of α and β tubulin, each monomer is comprised of approximately 450 amino acids, i.e., on the order of 7000 atoms. In the initial part of our calculations, we present results for the electrostatic potential in vacuum surrounding the protein. Later on, we discuss the effects of solvent with ions.

Nogales *et al.* [9] imaged tubulin heterodimers to atomic resolution establishing that, the structures of α and β tubulin are nearly identical and confirming the consensus speculation. A detailed examination shows that, each monomer is formed by a core of two β-sheets that are surrounded by α-helices. The monomer structure is very compact, but can be divided into three functional domains: the amino-terminal domain containing the nucleotide binding region, an intermediate domain containing the taxol binding site, and the carboxy-terminal domain, which probably constitutes the binding surface for motor proteins.

Calculations of the potential energy were done with the aid of a molecular dynamics package, TINKER [14]. This computer program serves as a platform for molecular dynamics simulations and includes the facility to use several force-field parameter sets, some of which are protein specific. The most common of these parameter sets for proteins are AMBER [15] and CHARMM [16]. AMBER was selected over CHARMM on the rationale that it is a more up-to-date parameter set. The overall performance of the program gave us confidence that the results it provided for tubulin were meaningful. It was determined using TINKER that tubulin is quite highly negatively charged at physiological pH and that much of the charge is concentrated on the C-terminus. (Perhaps as much as 40% of the overall charge.)

Figure 4 shows an experimental titration curve for the net charge on the tubulin $\alpha\beta$ heterodimer (with the C-termini) as a function of pH. We have also been able to obtain a detailed map of the electric charge distribution on the surface of the tubulin dimer (see Figure 5). It is clear that, the

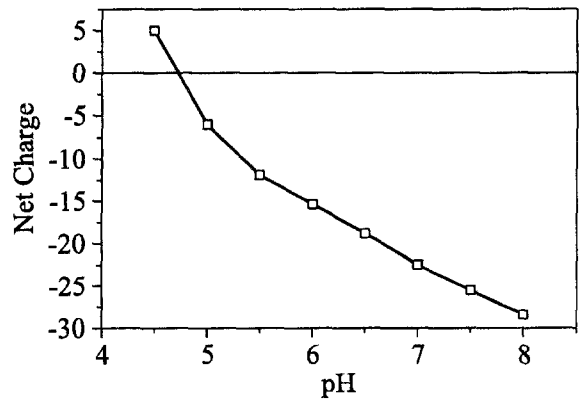

Figure 4. Tubulin titration curve for the tubulin $\alpha\beta$ heterodimer as a function of pH; obtained with no salt and no intra-molecular charge compensation. Figure courtesy of Sackett [17].

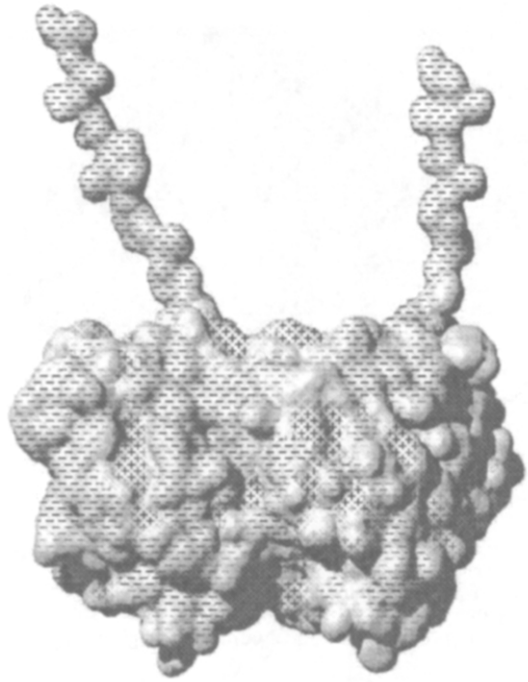

Figure 5. A map of the electric charge distribution on the surface of a tubulin dimer with C-termini tails present. Figure prepared using MOLMOL [18].

C-termini which extend outward carry a significant electric charge. At neutral pH, the negative charge on the carboxy-terminus causes it to remain extended due to the electrostatic repulsion within the tail. Under more acidic conditions, the negative charge of the carboxy-terminal region is reduced by associated hydrogen ions. The effect is to allow the tail to acquire a more compact form by folding (see Figure 6). Although this is probably the largest structural effect which occurs due to changes in the cell's pH, we expect that other structural changes, perhaps the result of post-translational modifications in the process of microtubule assembly, can similarly affect the electrostatics of the tubulin dimer.

In Figure 7, we have constructed a hydrophobicity map showing the location of hydrophobic and hydrophilic regions in the α tubulin monomer. In it, regions of dark minus signs are strongly hydrophobic, the lighter ones less so while increasingly dark plus signs correspond to an increasing level of hydrophylicity.

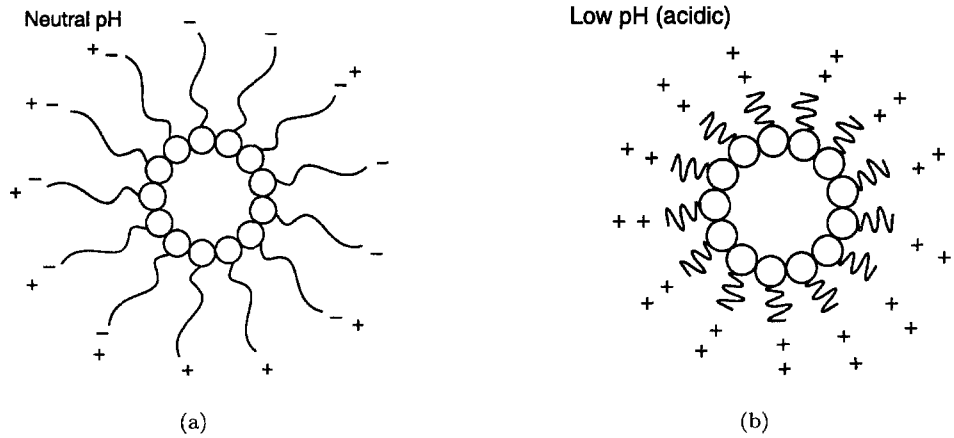

Figure 6. Cross-section of a MT including the carboxy-termini of the tubulin subunits. The folding shown of the carboxy-termini of the tubulin dimer demonstrates the change in the geometry of the molecule with pH. Neutral pH is shown on top, the tail folds at lower pH as the negative charges are screened.

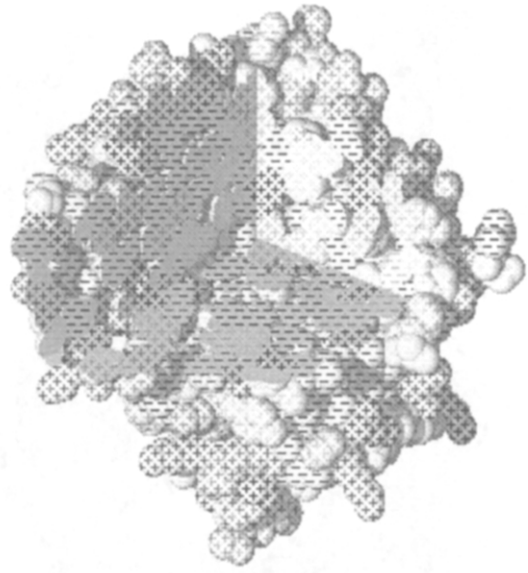

Figure 7. A cut-open view of the α-monomer of tubulin illustrating the location of hydrophobic regions (minus signs) and hydrophilic regions (plus signs).

In Figure 8a, we have imaged the electrostatic potential inside the tubulin dimer. It is interesting to note that, the hydrophobic interior of the protein gives rise to a nicely symmetric electrostatic potential with the different rings indicating equipotential surfaces. While the topography of the potential slices taken in the plane perpendicular to the dimer axis is, for the most part, concentric, towards the top layer of the dimer the sampled cross-sections reveal a double-well structure. This may indicate that charged groups present in this region could execute tunneling motions between the two equivalent energy minima. A close-up view of one such cross-section is given in Figure 8b.

In Table 1, we listed the dipole moment of the dimer without the tails (see Figure 9a). The story here, however, is more complicated. As shown in Figure 9, there are several additional sources of dipoles when tubulin is present in an ionic solution. When two dimers are bound within a protofilament, their positively and negatively charged ends form a double layer with a net dipole moment along the protofilament axis (Figure 9b). Beside each tubulin monomer there is a hydrophobic pocket that may develop a double-well structure (see Figure 8). This can give rise to an internal (switchable) dipole moment due to electronic transitions on this positive

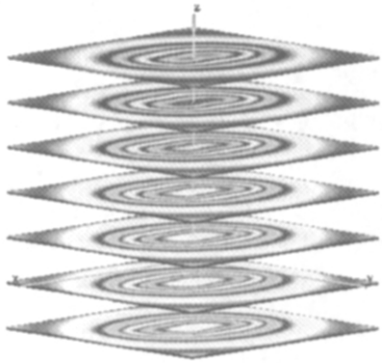

(a) Cross-section slicing perpendicular to its axis.

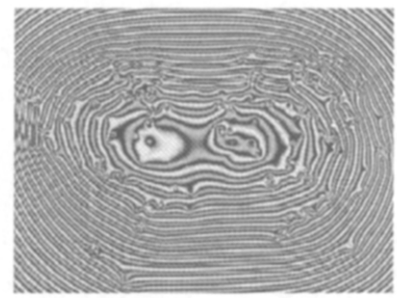

(b) A double-well potential region close to the top of the $\alpha - \beta$ heterodimer.

Figure 8. Images of the electrostatic potential inside a tubulin dimer.

Table 1. Tubulin's electrostatic properties (tail region excluded)[a].

Tubulin Properties	Dimer	α Monomer
Charge (Electron Charges)	−10	−5
dipole (Debyes)		
overall	1714	566
P_x component	337	115
P_y component	−1669	−554
P_z component	198	−6

[a] The x-direction coincides with the protofilament axis. The α monomer is in the direction of increasing x values relative to the β monomer. The y-axis is oriented radially towards the MT centre and the z-axis is tangential to the MT surface.

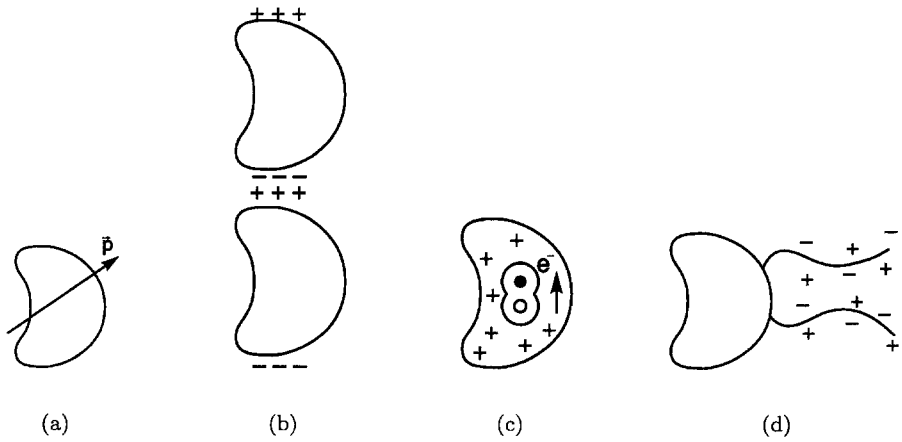

Figure 9. The various contributions to the dipole moment of a tubulin dimer (a) the intrinsic dipole moment of the globular protein, (b) the double layer formed when two dimers are bound in a protofilament, (c) a possible internal dipole created by electronic transitions in the hydrophobic pocket, and (d) a double layer formed by counter ions surrounding the C-termini tails.

background (see Figure 9c). Finally, as is shown in Figure 9d the C-termini which are negatively charged are surrounded by counter ions in solution leading to the formation of double layers. The principal contribution to the dipole moment of a tubulin dimer comes, however, from the location of partial charges on the constituent amino acids.

3. ELECTROSTATIC POTENTIAL AROUND TUBULIN

Having obtained the charge distribution on the tubulin surface, we have attempted to investigate its role in the microtubule lattice formation and its interaction with ions and macromolecules. We have confined our examination largely to the surfaces of tubulin that form the exterior surface and the protofilament-protofilament contacts when assembled into a MT. The first result that may be derived from the electrostatic potential is that there are those regions of the MTs outer surface that are negatively charged and which may attract hydrogen ions.

In calculating the electrostatic potential, 2.0 nm was selected as the cutoff distance for charge, dipole, and van der Waal interactions. The electrostatic potential was calculated for a 12 nm segment of the line, thereby including an additional 2 nm above and below each tubulin molecule. Periodic boundary conditions were then applied in the direction of the protofilament because this is the configuration of the tubulin dimers within a MT. The resulting profiles of the electrostatic potential are shown in Figure 10 and are located about the tubulin dimer as shown in Figure 11. The lateral boundary conditions were not considered in the calculation of the potential.

Consider the profile of the electrostatic potential in Figures 10a and 10b and compare them with the profiles in Figures 10c and 10d. These are left and right sides, respectively, of the

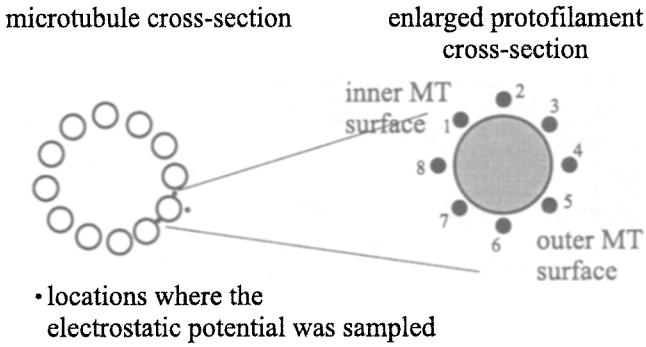

Figure 10. A MT cross-section illustrates where the electrostatic potential was examined along lines parallel to the protofilament axis (perpendicular to the page) in the preceding figure.

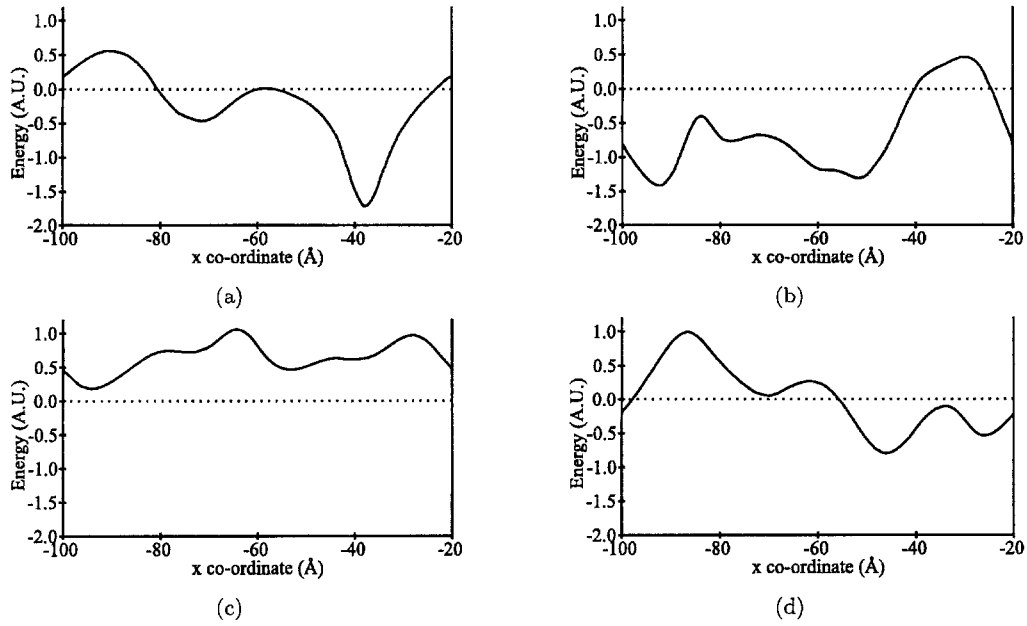

Figure 11. Electrostatic profiles along lines parallel to the protofilament axis. (a) Line 3-MTs interior on the A side of the protofilament-protofilament interface. (b) Line 4-MTs exterior on the A side of the protofilament-protofilament interface. The profile is largely negative indicating the negative surface charge. (c) Line 7-MTs exterior on the B side of the protofilament-protofilament interface. The largely positive surface charge is complementary to the opposite side of the dimer and contributes to protofilament-protofilament binding. (d) Line 8-MTs exterior on the B side of the protofilament-protofilament interface.

tubulin molecule, which interact laterally to hold one protofilament together with neighboring protofilaments. In these figures, each unit of energy represents 14.4 kcal/mol or 0.62 eV. This is roughly the energy available from the hydrolysis of two to three molecules of GTP or just a little more than the hydrolysis of one molecule of ATP. What is interesting is that, the electrostatic potential is largely negative on the left side and positive on the right side. Thus, there is a net electrostatic attraction between tubulin dimers with parallel alignment when their opposite sides face each other. In fact, if the minima in the left side's profile are aligned with the maxima in the electrostatic potential of the right side, we find that the neighboring tubulin dimer will be shifted by 1.4 nm or 5.4 nm which compares reasonably well to the observed 0.9 nm or 4.9 nm offsets that depend on the lattice type. The simple change of a residue on the surface offers the possibility of specifying one shift and locking the resulting MT into either the A or B type lattice. Hence, post-translational modification or more likely the expression of a particular isotype over another could select a specific lattice.

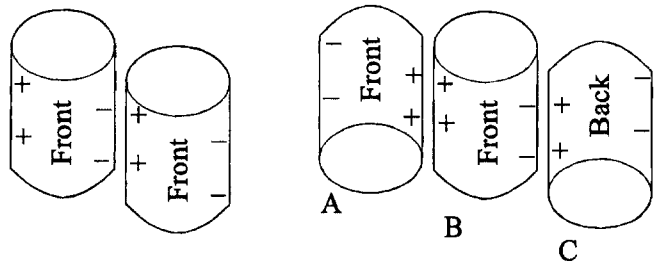

Figure 12. Protofilament-protofilament interaction. At left, tubulin dimers associate such that there is a vertical offset between protofilaments. At right, when the dimer's up-down orientation is reversed, it must also be rotated from front to back since the interaction between A and B is destabilizing but the interaction between B and C is stabilizing.

In the event that, we wish to consider tubulin aggregations such as the zinc(II) ion-induced sheets that were prepared in the tubulin structure determination experiments [9], the protofilaments have an anti-parallel configuration. As a result, proceeding on the premise that electrostatic interactions determine the protofilament-protofilament binding, the zinc(II) ion must work to alter this interaction. Since, the pattern of the electric potential consisting of two electrostatic wells on one side and two electrostatic peaks on the opposite side must be maintained, to explain the efficient binding of the dimers into the lattice of the tubulin sheet or MT, the potential is presumably not tremendously distorted. Since each tubulin dimer will be affected in the same manner, forming anti-parallel protofilaments does require that either the energy profile changes such that each side has a well and peak in the potential or conversely, that there is a small change in the potential which now favors binding where the "front" of the tubulin dimer is presented to an observer along protofilaments with the first orientation while the "back" of the tubulin dimer faces the observer for the protofilaments with the opposite orientation (see Figure 12).

4. ELECTROSTATIC EFFECTS OF MICROTUBULE STRUCTURE

When the previous investigations of the electrostatics of tubulin are brought to bear on the structure of the microtubule, we predict the emergence of a very unusual anti-ferroelectric structure. This is shown in Figure 13 with tubulin's permanent dipoles placed almost perpendicular to the surface of the microtubule cylinder and almost canceling one another due to rotational symmetry. It is tantalizing to speculate that such a dipolar structure may be constructed to facilitate the docking process of motor proteins such as kinesin. Bearing in mind that tubulin is

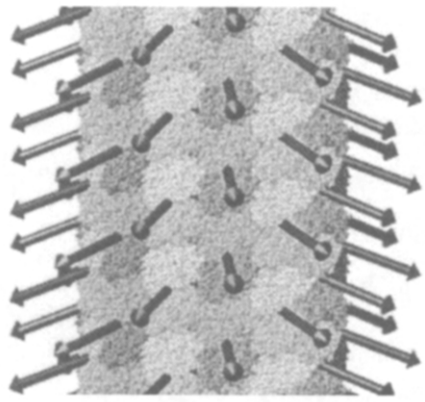

Figure 13. The arrows indicate the orientation of the permanent dipole moments of individual tubulin dimers with respect to the surface of a microtubule. Figure prepared using MOLMOL [18].

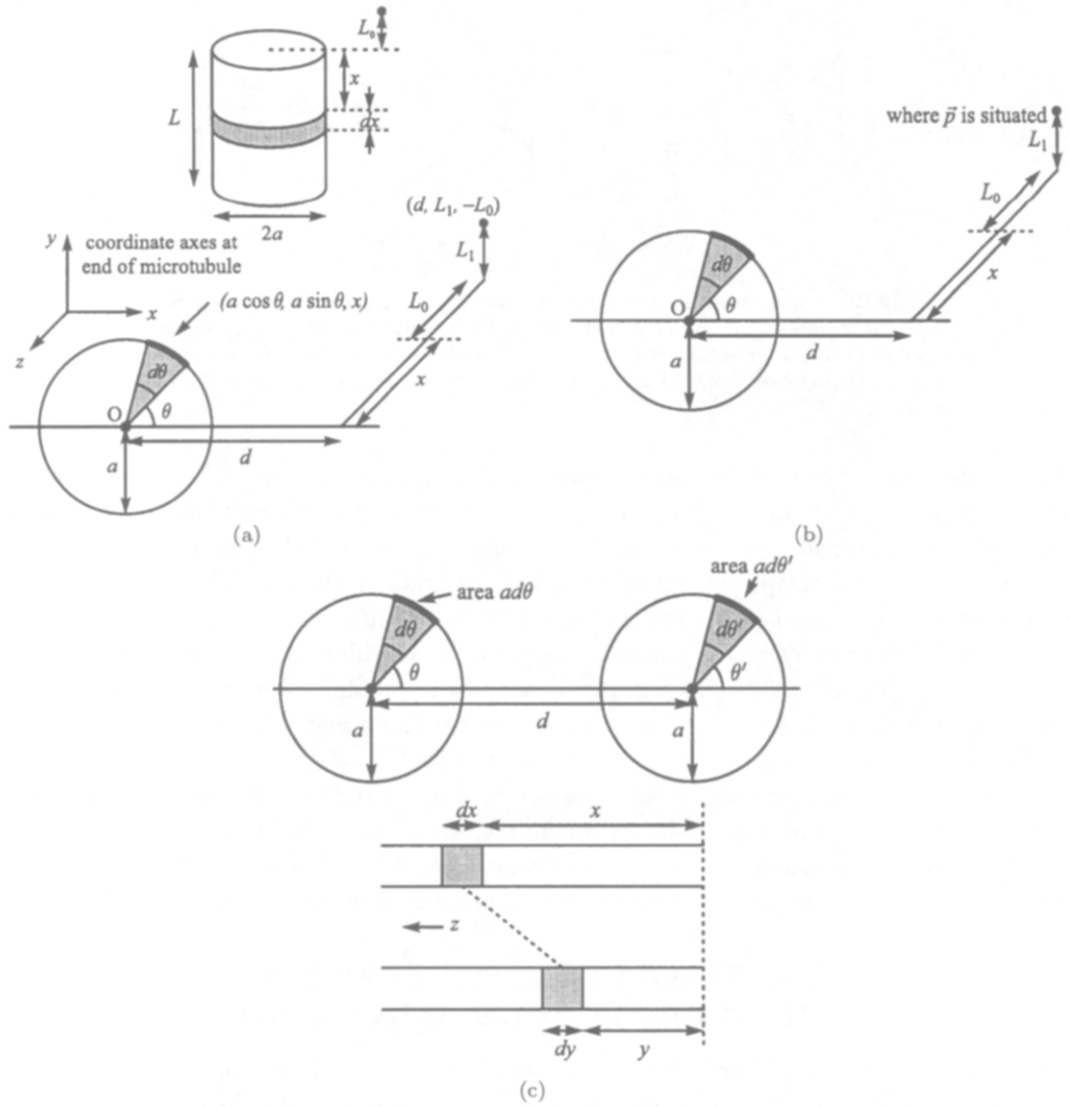

Figure 14. Geometrical arrangements for the calculations of (a) test charge-microtubule interaction; (b) test dipole-microtubule interaction; and (c) the interaction between two parallel microtubules.

both highly charged and possesses a permanent dipole moment we have attempted to estimate the strength of electrostatic effects on,

(a) a test charge,
(b) a test dipole,
(c) another microtubule in the vicinity, and
(d) the dipole-dipole interaction between two microtubules.

Below, we summarize our calculations and Figure 14 illustrates the geometrical details.

A. Microtubule-Charge Interaction

Consider a microtubule with charge per unit area σ on its surface, with a length L, and a diameter $2a$. Suppose a point charge is situated at the points $(d, L_1, -L_0)$ relative to the origin as shown in Figure 14a. We calculate the electric field intensity at the point-charge location assuming the electrical relative permittivity to be ε. Using the formula

$$E = \int_0^L \int_0^{2\pi} \frac{\sigma a \, d\theta \, dx}{4\pi\varepsilon_0\varepsilon(d^2 + a^2 - 2ad\cos\theta - 2aL_1\sin\theta + L_1^2 + (x + L_0)^2)}, \tag{4.1}$$

we assume $d \gg a$ so that $d^2 + a^2 + L_1^2 + (x + L_0)^2$ is much greater than the terms in ad and aL_1. In the angular part of the integration we retain the leading term only and find that

$$E \approx \frac{\sigma a}{2\varepsilon_0 \varepsilon} \frac{1}{\sqrt{d^2 + a^2 + L_1^2}} \left[\tan^{-1} \left(\frac{L + L_0}{\sqrt{d^2 + a^2 + L_1^2}} \right) - \tan^{-1} \left(\frac{L_0}{\sqrt{d^2 + a^2 + L_1^2}} \right) \right]. \tag{4.2}$$

For sufficiently long microtubules

$$E \approx \frac{\sigma a}{2\varepsilon_0 \varepsilon} \frac{1}{\sqrt{d^2 + a^2 + L_1^2}}. \tag{4.3}$$

The results presented for the electrostatic potential in this paper represent "vacuum" results given that, the solvent is not explicitly taken into account. If the surrounding mixture of ions is considered, then the potential due to a point charge does not fall off simply as $1/r$ but instead as $\phi \propto (1/r)e^{-K(r-r_0)}$ where K^{-1} is the Debye length, typically close to 1 nm under physiological conditions [19]. The constant r_0 is the ionic radius. Since we consider locations within several nanometers of the MT surface, they are not completely screened by the ions of the solution.

As an example consider an average length of the microtubule of $L = 5\,\mu$m, $a = 12.5$ nm, and $\sigma = 0.5\,\mathrm{e/nm^2}$ which is consistent with our earlier discussion. With a test charge of $+5$ e located with $L_1 = 0$ and distance 5 nm from the surface we obtain a force of electrostatic attraction of 6 pN in water which is reduced to only 0.5 pN in standard ionic solution with a Debye length of 0.6–1.5 nm depending on the ionic strength. This would indicate that, the maximum distance over which a microtubule can exert an influence on a charged particle is on the order of 5 nm from its surface.

B. Microtubule-Dipole Interaction

Here, we consider a microtubule with a dipole moment per unit area, σ_D, on its surface, each dipole moment being perpendicular to its surface. The test dipole is assumed to be at the point $(d, +L_1, -L_0)$ as we illustrate in Figure 14b. The distance between this latter dipole and a dipole on a small element of area $\sigma_D a\, d\theta\, dx$ at $(a\cos\theta,\, a\sin\theta, x)$ is given by

$$\sqrt{(a\cos\theta - d)^2 + (a\sin\theta - L_1)^2 + (L_0 + x)^2}. \tag{4.4}$$

As a result the test dipole, with dipole moment $\vec{p}$, has a dipolar energy H_E, due to its interaction with the microtubule, given by

$$H_E = \sigma_D \int_0^L \int_0^{2\pi} \frac{a\, d\theta\, dx \left[\hat{n} \cdot \vec{p} - 3\,(\vec{n} \cdot \hat{n})\,(\vec{n} \cdot \vec{p})\right]}{4\pi\varepsilon_0 \varepsilon \left(d^2 + a^2 - 2ad\cos\theta - 2aL_1 \sin\theta + L_1^2 + (x + L_0)^2\right)^{3/2}}, \tag{4.5}$$

where $\hat{n}$ is a unit vector in the direction of the dipole moment of the element of area on the microtubule. That is

$$\hat{n} = \hat{\imath}\cos\theta + \hat{\jmath}\sin\theta. \tag{4.6}$$

Here, $\hat{\imath}$ and $\hat{\jmath}$ are unit vectors along the x and y coordinate axes. On the other hand, $\vec{n}$ is a unit vector along the direction from the surface element to the location of the test dipole. Hence,

$$\vec{n} = \frac{(a\cos\theta - d)\hat{\imath} + (a\sin\theta - L_1)\hat{\jmath} + (L_0 + k)\hat{k}}{\sqrt{(a\cos\theta - d)^2 + (a\sin\theta - L_1)^2 + (L_0 + x)^2}}, \tag{4.7}$$

where $\hat{k}$ is a unit vector along the z coordinate axis parallel to the length of the microtubule. The angular integral in equations (4.5) is evaluated by taking only the leading terms (since on

expansion, using the approximations in Section 4a, terms in $\sin\theta$ and $\cos\theta$ will vanish). Denoting the x, y, and z components of the test dipole by p_x, p_y, and p_z we find

$$\begin{aligned} H_E \approx & \frac{a\sigma_D}{4\pi\varepsilon_0\varepsilon\gamma} \frac{12ad\pi p_x + 12aL_1\pi p_y}{\left(d^2+a^2+L_1^2\right)^2} \\ & \times \left[\sin\left(\tan^{-1}\left(\frac{L+L_0}{\sqrt{d^2+a^2+L_1^2}}\right)\right) - \frac{1}{3}\sin^3\left(\tan^{-1}\left(\frac{L+L_0}{\sqrt{d^2+a^2+L_1^2}}\right)\right)\right. \\ & \left. - \sin\left(\tan^{-1}\left(\frac{L_0}{\sqrt{d^2+a^2+L_1^2}}\right)\right) + \frac{1}{3}\sin^3\left(\tan^{-1}\left(\frac{L_0}{\sqrt{d^2+a^2+L_1^2}}\right)\right)\right] \\ & + a^2\sigma_D 2\pi p_z \left(\left(d^2+a^2+L_1^2+(L+L_0)^2\right)^{-3/2} - \left(d^2+a^2+L_1^2+L^2\right)^{-3/2}\right). \end{aligned} \tag{4.8}$$

Note that, for an infinite cylindrical dipole surface with a uniform value of the dielectric constant in all space, the potential at an arbitrary point in space exterior to the cylinder is zero. However, here we deal with a finite cylinder. More importantly, there is a large difference between the dielectric constant in the medium (close to 80 for H_2O) and inside the protein (in the range of 2 to 4). Since interactions of a test dipole with the layer facing it are through the medium only while those with the layer turned away from it also involve a large portion of the space filled with protein, there will be a non-zero result. For distances comparable to the MT diameter we have introduced an appropriate correction parameter γ which varies between 2 and 3 depending on the distance. We have used the dielectric constant of water for ε.

To get a sense of energies involved in the interaction between a polar molecule in solution and a microtubule a distance of 5 nm away, we consider a 5 μm microtubule whose tubulin dimers possess a dipole moment on the order of 2000 D each, the latter may include an additional contribution from a double layer of water and ions. Assume first that a macromolecule carrying a dipole moment of 200 D along the x axis is situated in the equatorial plane of the cylinder where $L_1 = L_0 = 0$. Using equation (4.8) we obtain the energy of the dipole-dipole interaction, in this case to be a disappointing 0.03 meV which is much less than the energy of thermal fluctuations. However, repeating this calculation for a fictitious tubulin dimer in solution whose 2000 D dipole moment is oriented along the y axis and which is located so that $L_1 = 1\,\mu$m above the plane, everything else remaining the same as before (with $\gamma = 3$), we find that the interaction energy is now just above 2 meV—a value smaller than room temperature thermal fluctuations. Clearly, this indicates a minimal role of the dipolar structure of microtubules in promoting orientational order. This effect may become significant, however, as the assembling molecule approaches the surface for docking both on account of short distances and the decreasing dielectric constant [19]. Notice that, it transpires from equation (4.8) that, the interaction with the z-component of the dipole (which is along the microtubule axis) is very small.

C. Charged Microtubule-Charged Microtubule Interaction

In this section, we consider the force of interaction between the charge distributions, assumed uniform, on two parallel microtubules. We assume there is a charge σ per unit area on each, and consider two elements of area $a\,d\theta\,dx$ and $a\,d\theta'\,dy$, respectively. The square of the distance between the elements (see Figure 14c) is given by $(x-y)^2 + D^2$ where $D^2 = (a\sin\theta - a\sin\theta')^2 + (d - a\cos\theta - a\cos\theta')^2$. The force, F_1, is given by

$$F_1 = \int_0^{2\pi}\int_0^{2\pi}\int_0^{L}\int_0^{L} \frac{\sigma^2 a^2}{4\pi\varepsilon_0\varepsilon\left[(x-y)^2+D^2\right]}\,dx\,dy\,d\theta\,d\theta'. \tag{4.9}$$

Assuming that $d^2 + (x-y)^2$ is very much greater than the other terms in the denominator of equation (4.9) we may expand and retain only leading terms in $\sin\theta, \cos\theta, \sin\theta'$, and $\cos\theta'$. When

integrated over θ and θ' these will vanish giving

$$F_1 \approx \int_0^L \int_0^L \frac{(2\pi)^2\sigma^2 a^2}{4\pi\varepsilon_0\varepsilon\left[(x-y)^2+d^2+2a^2\right]}\,dx\,dy. \tag{4.10}$$

We now change the variables from x, y to $z = x - y$ and $w = x + y$ with a Jacobian of $J = 1/2$. The integral part of equation (4.10), namely

$$I = \int_0^L \int_0^L \frac{dx\,dy}{(x-y)^2+d^2+2a^2}, \tag{4.11}$$

then becomes

$$I = \frac{1}{2}\int_0^L \int_{-w}^{w} \frac{dz\,dw}{z^2+d^2+2a^2} + \frac{1}{2}\int_L^{2L} \int_{w-2L}^{-w+2L} \frac{dz\,dw}{z^2+d^2+2a^2}. \tag{4.12}$$

The integrals in equation (4.12) then become elementary and therefore, F_1 is given by

$$F_1 \approx \frac{2\pi a^2\sigma^2}{\varepsilon_0\varepsilon}\left\{\frac{L}{\sqrt{d^2+2a^2}}\tan^{-1}\left(\frac{L}{\sqrt{d^2+2a^2}}\right) + \ln\left[\cos\left(\tan^{-1}\frac{L}{\sqrt{d^2+2a^2}}\right)\right]\right\}. \tag{4.13}$$

We have estimated this effect by using the same charge density as before and the length of each microtubule to be $5\,\mu$m. The distance between two neighboring microtubules cannot be less than 35 nm measuring it between the centres due to the repulsion between the C-termini. The force of repulsion in equation (4.13) for $d = 40$ nm in an aqueous environment is found to be staggering 0.2×10^6 pN. However, when Debye screening due to ions at a concentration of 150 nM is included the result is reduced to 9 pN. This is a significant number that may explain various ordering effects in microtubule bundles or asters.

D. Dipole-Dipole Interactions Between Two Microtubules

Consider the interaction between the dipole moment densities on two microtubules and suppose on each the dipole moment per unit area is σ_D. We consider an element on one microtubule with coordinates $(a\cos\theta, a\sin\theta, x)$ and an element at $(d + a\cos\theta', a\sin\theta', y)$ on the other. (The positioning of elements in space is the same as in Figure 14c.) Once again d is the distance between the axes of the microtubules which will be assumed parallel and a is their radius. The force between them becomes

$$F_2 = \int_0^L\int_0^L\int_0^{2\pi}\int_0^{2\pi} \frac{\sigma_D^2\left[\hat{n}_x\cdot\hat{n}_y - 3\left(\vec{n}\cdot\hat{n}_x\right)\left(\vec{n}\cdot\hat{n}_y\right)\right]d\theta'\,d\theta\,dy\,dx}{4\pi\varepsilon_0\varepsilon\gamma^2\left[(x-y)^2+\left(a\sin\theta-a\sin\theta'\right)^2+\left(d+a\cos\theta'-a\cos\theta\right)^2\right]^2}, \tag{4.14}$$

where $\vec{n}$ is a unit vector along the line joining the two elements and given by

$$\vec{n} = \frac{\left(d+a\cos\theta'-a\cos\theta\right)\hat{\imath}+\left(a\sin\theta'-a\sin\theta\right)\hat{\jmath}+(y-x)\hat{k}}{\left[\left(d+a\cos\theta'-a\cos\theta\right)^2+\left(a\sin\theta'-a\sin\theta\right)^2+(y-x)^2\right]^2}. \tag{4.15}$$

The unit vector $\hat{n}_x$ denotes the direction of the dipole moment on the element at $(a\cos\theta, a\sin\theta, x)$ so, that $\hat{n}_x = \cos\theta\hat{\imath} + \sin\theta\hat{\jmath}$.

The direction of the dipole moment on the element at $(d + a\cos\theta', a\sin\theta', y)$ is defined by the unit vector

$$\hat{n}_y = \frac{\left(d+a\cos\theta'\right)\hat{\imath}+a\sin\theta'\hat{\jmath}}{\sqrt{\left(d+a\cos\theta'\right)^2+\left(a\sin\theta'\right)^2}}. \tag{4.16}$$

Assuming that, the square in equation (4.14) may be expanded by factoring out $(x-y)^2+d^2+2a^2$, similarly in equation (4.15) and extracting d^2+a^2 in equation (4.16) we have linearized and retained leading terms as we did in Section 4c. This is done by first performing the angular integrals and then dropping all denominators which involve $(x-y)^2+d^2+2a^2$, d^2+a^2, and $[(x-y)^2+d^2+2a^2][d^2+a^2]$ which we assume are small. The net result is that the force, F_2, becomes

$$F_2 \approx \frac{a^2\sigma_D^2}{4\pi\varepsilon_0\varepsilon\gamma^2}\frac{-2ad^2\pi^2}{\sqrt{d^2+a^2}}\int_0^L dx\int_0^L \frac{dy}{\left((x-y)^2+2a^2+d^2\right)^3}. \tag{4.17}$$

The integrals now become tractable if we change variables again to $z=x-y$ and $w=x+y$. We find that, the resultant force is

$$\begin{aligned} F_2 \approx & \frac{a^3\sigma_D^2 d^2\pi}{\varepsilon_0\varepsilon\gamma^2\sqrt{d^2+a^2}\left(d^2+2a^2\right)^2} \\ & \times\left\{\frac{3}{8}\frac{L}{\sqrt{d^2+2a^2}}\tan^{-1}\left(\frac{L}{\sqrt{d^2+2a^2}}\right)+\frac{1}{8}\sin^2\left[\tan^{-1}\left(\frac{L}{\sqrt{d^2+2a^2}}\right)\right]\right\}. \end{aligned} \tag{4.18}$$

Taking as before the polarization density of 2000 D per dimer and a separation between microtubule centres to be 40 nm and using $L=5\,\mu$m as well as $\gamma=3$ results in the attractive force, F_2, between the two microtubules of 330 pN which is very significant. Moving the distance between microtubules to 90 nm (which is the mean separation between axonal microtubules) reduces the attraction force by a factor of 4000 to a mere 0.08 pN. It is also worth emphasizing that a combined action of monopole-monopole and dipole-dipole forces will have a competitive nature with Coulomb repulsion on short distances due to negative charges of the microtubular surfaces and an attractive dipole-dipole interaction that evidently extends over a larger range. Hence, it is expected that an equilibrium distance between neighboring microtubules may be established as a global energy minimum.

5. DISCUSSION AND CONCLUSION

In this paper, we have summarized our calculations regarding the net charges and dipole moments of tubulin and microtubules. These calculations were performed using an atomic resolution structure of tubulin in conjunction with molecular dynamics simulations. We found a large negative charge concentrated on the outer surface of the protein, almost half of which is located on flexible peptide tails attached to the outer face. This charge is undoubtedly instrumental in tubulin-tubulin interactions as well as the interactions of tubulin with motor proteins such as kinesin. Figure 15 shows the results of our force field calculations where two tubulin dimers are placed in each other's neighborhood and allowed to interact electrostatically. The brush strokes represent the direction of the Coulomb force of attraction.

We have also shown that, the microtubule structure, in particular the lateral binding between protofilaments, is consistent with the location of positive and negative segments of the electrostatic potential for optimal binding. It is worth mentioning that, a recent paper [20] showed the electrostatic surface of the whole microtubule following computations involving the Poisson-Boltzmann equation. From these calculations a dramatic difference between the plus and minus ends of a microtubule has been revealed. It is very likely that, this difference leads to the well-known difference is polymerization kinetics involving these two ends. In our paper, we have also considered the role of electrostatics in the interactions between microtubules and other charged or polarized molecules. In particular, in spite of Debye screening, a microtubule can exert a Coulomb force on a charged particle that is up to 5 nm away from its surface. The dipole-dipole forces that have been found are negligible for the most part. However, they can be felt by dipoles that are perpendicular to the microtubule surface and removed from the equatorial plane. When two microtubules are found in the same vicinity, they can exert significant forces of repulsion even

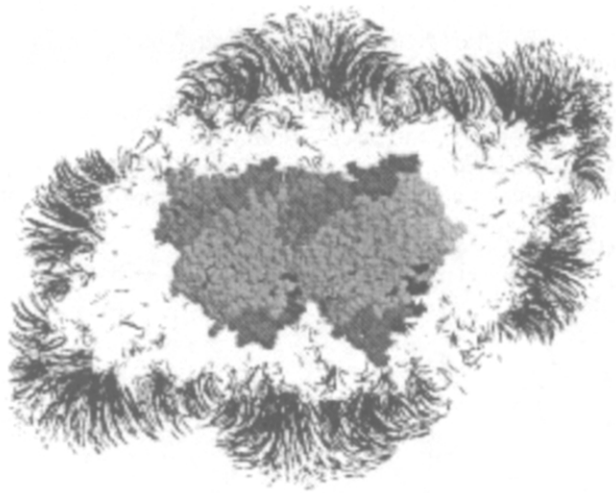

Figure 15. A view of the attractive regions about a tubulin dimer as would be experienced by another dimer. The smallest principal moment of inertia of the dimers is perpendicular the page, the middle one is aligned vertically, the largest principal moment horizontally. See, text for more details. Figure prepared using [11].

in the presence of ionic screening. Since the negatively charged C-termini protrude perpendicularly to the microtubule surface this effect is additionally increased and explains the existence of the so-called "zone of exclusion" [21].

In conclusion, our calculations demonstrate a significant role played by charge and dipole forces in both the formation of microtubules and their interactions with other proteins and possibly drug molecules. The latter observation may lead to a fruitful search for microtubule binding drugs such as derivatives of taxol. In addition, there has already been progress in understanding cell division by the inclusion of electrostatic interaction mechanisms as shown in a recent paper [22].

REFERENCES

1. M.C. Ledbetter and K.R. Porter, A "microtubule" in plant cell fine structure, *Journal of Cell Biology* **19** (1), 239–250, (1963).
2. D. Chrétien, S.D. Fuller and E. Karsenti, Structure of growing microtubule ends: Two-dimensional sheets close into tubes at variable rate, *Journal of Cell Biology* **129** (5), 1311–1328, (1995).
3. L.A. Amos and W.B. Amos, *Molecules of the Cytoskeleton*, First Edition, MacMillan Press, London, (1991).
4. D. Chrétien and R.H. Wade, New data on the microtubule surface lattice, *Biology of the Cell* **71** (1–2), 161–174, (1991).
5. L.A. Amos, The microtubule lattice—20 years on, *Trends in Cell Biology* **5** (2), 48–51, (1995).
6. D. Chrétien, F. Metoz, F. Verde *et al.*, Lattice defects in microtubules: Protofilament numbers vary within individual microtubules, *Journal of Cell Biology* **117** (5), 1031–1040, (1992).
7. H. Sosa and R.A. Milligan, Three-dimensional structure of NCD-decorated microtubules obtained by a back-projection method, *Journal of Molecular Biology* **260** (5), 743–755, (1996).
8. M.V. Semënov, New concept of microtubule dynamics and microtubule motor movement and new model of chromosome movement in mitosis, *Journal of Theoretical Biology* **179** (2), 91–117, (1996).
9. E. Nogales, S.G. Wolf and K.H. Downing, Structure of the alpha-beta tubulin dimer by electron crystalography, *Nature* **393** (6663), 199–203, (1998).
10. H.M. Berman, J. Westbrook, Z. Feng *et al.*, The protein data bank, *Nucleic Acids Research* **28** (1), 235–242, (2000).
11. R.A. Sayle and E.J. Milner-White, RasMol: Biomolecular graphics for all, *Trends in Biochemical Sciences* **20** (9), 374–376, (1995).
12. Q. Lu, G.D. Moore, C. Walss *et al.*, Structural and functional properties of tubulin isotypes, *Advances in Structural Biology* **5**, 203, (1998).
13. P.G. Wilson and G.G. Borisy, Evolution of the multi-tubulin hypothesis, *Bioessays* **19** (6), 451–454, (1997).
14. M.J. Dudek and J.W. Ponder, Accurate modelling of the intramolecular electrostatic energy of proteins, *Journal of Computational Chemistry* **16** (7), 791–816, (1995).
15. D.A. Pearlman, D.A. Case, J.W. Caldwell *et al.*, AMBER, a package of computer programs for applying molecular mechanics, normal mode analysis, molecular dynamics and free energy calculations to simulate the structural and energetic properties of molecules, *Computer Physics Communications* **91**, 1–41, (1995).

16. B.R. Brooks, R.E. Bruccoleri, B.D. Olafson *et al.*, CHARMM: A program for macromolecular energy, minimization, and dynamics calculations, *Journal of Computational Chemistry* **4** (2), 187–217, (1983).
17. D.L. Sackett, Personal communication (2000).
18. R. Koradi, M. Billeter and K. Wüthrich, MolMol: A program for display and analysis of macromolecular structures, *J. Mol. Graphics* **14** (1), 51–55, 29–32, (1996).
19. M. Daune, *Molecular Biophysics: Structures in Motion*, Oxford University Press, (1999).
20. N.A. Baker, D. Sept, S. Joseph *et al.*, Electrostatics of nanosystems: Application to microtubules and the ribosome, *Proc. Nat. Acad. Sci.* **98** (18), 10037–10041, (2001).
21. P. Dustin, *Microtubules*, Springer-Verlag, Berlin, (1984).
22. L.J. Gagliardi, Electrostatic force in prometaphase and anaphase—a chromosome motions, *Phys. Rev. E* **66**, 011 901, (2002).